Supporting Information

General Route to Design Solar Thermoelectric Generators under the Constant Heat Flux Thermal Boundary

Huan Li[1], Yupeng Wang[1], Xinzhi Wu[1], Kang Zhu[2], Shuaihua Wang[1], Mao Yu[1], Weishu Liu[1,*]

[1] Department of Materials Science and Engineering, Southern University of Science and Technology, Shenzhen, Guangdong 518055, China

[2] School of Advanced Energy, Sun Yat-sen University, Shenzhen, Guangdong 518107, China

[*] Corresponding Author

ORCID iD: 0000-0001-8643-822X

Phone number: 0755-88018955

Email: liuws@sustech.edu.cn

Huan Li: 12132046@mail.sustech.edu.cn

Yupeng Wang: 12131019@mail.sustech.edu.cn

Xinzhi Wu: 12031208@mail.sustech.edu.cn

Kang Zhu: zhuk36@mail.sysu.edu.cn

Shuaihua Wang: 12132079@mail.sustech.edu.cn

Mao Yu: 12232090@mail.sustech.edu.cn

Note S1. Derivation of the efficiency model for STEGs

To facilitate the derivation of equations, we assumed that thermoelectric properties are temperature-independent, and the Thomson coefficient becomes zero. Therefore, according to the governing equation deduced in Liu's work[1, 2] and boundary conditions, the governing model for STEG is shown as follows

$$\begin{cases} \kappa \dfrac{d^2T(x)}{dx^2} + \dfrac{I^2}{\sigma A^2} = 0 & (a) \\ Q_{\mathrm{h}} = ST(x)I - (A\kappa + A_{\mathrm{i}}\kappa_i)\dfrac{dT}{dx} + \dfrac{T(x) - T_{\mathrm{a}}}{R_{\mathrm{h}}}, x = 0 & (b) \\ ST(x)I - (A\kappa + A_{\mathrm{i}}\kappa_i)\dfrac{dT}{dx} = \dfrac{T(x) - T_{\mathrm{a}}}{R_{\mathrm{c}}}, x = h & (c) \end{cases} \tag{S1}$$

where κ is the thermal conductivity, T is the temperature, x is the distance along the thermoelectric leg, I is the current, σ is the electric conductivity, A is the area of the thermoelectric leg, Q_{h} is the input heat, S is the Seebeck coefficient, A_{i} is the area of insulation material, κ_{i} is the thermal conductivity of insulation material, T_{a} is the ambient temperature, R_{h} is the hot-side thermal resistance, R_{c} is the cold-side thermal resistance. For convenience, we used f_{h}, f_{c}, and f_{i} to represent the influence caused by hot-side, cold-side, and insulation thermal resistance, respectively. The three variables are expressed as follows

$$f_{\mathrm{h}} = \frac{R_{\mathrm{h}}}{R_{\mathrm{t}}} \tag{S2}$$

$$f_{\mathrm{c}} = \frac{R_{\mathrm{c}}}{R_{\mathrm{t}}} \tag{S3}$$

$$f_{\mathrm{i}} = \frac{A\kappa}{A_{\mathrm{i}}\kappa_i} = \frac{R_{\mathrm{i}}}{R_{\mathrm{t}}} \tag{S4}$$

where R_{i} and R_{i} are the thermal resistance of the thermoelectric leg and insulation material, respectively. Since the filling material is generally the same height as the thermoelectric leg, f_{i} not only represents $A\kappa$ and $A_{\mathrm{i}}\kappa_{\mathrm{i}}$ but also represents the ratio of R_{i} to R_{t}. Then, substitute Equations (S2), (S3), and (S4) into Equation (S1).

$$\begin{cases} \kappa \dfrac{d^2T}{dx^2} + \dfrac{I^2}{\sigma A^2} = 0 & (a) \\ Q_{\mathrm{h}} = ST(x)I - A\kappa\left(1+\dfrac{1}{f_{\mathrm{i}}}\right)\dfrac{dT}{dx} + \dfrac{T(x)-T_{\mathrm{a}}}{f_{\mathrm{h}}R_{\mathrm{t}}}, x=0 & (b) \\ ST(x)I - A\kappa\left(1+\dfrac{1}{f_{\mathrm{i}}}\right)\dfrac{dT}{dx} = \dfrac{T(x)-T_{\mathrm{a}}}{f_{\mathrm{c}}R_{\mathrm{t}}}, x=h & (c) \end{cases} \tag{S5}$$

To further derive, the definition of R_{t} and electric resistance of thermoelectric leg (R_{e}) need to be shown as follows

$$R_{\mathrm{t}} = \frac{h}{A\kappa} \tag{S6}$$

$$R_{\mathrm{e}} = \frac{h}{A\sigma} \tag{S7}$$

Then, substitute Equations (S6) and (S7) into Equation (S5).

$$\begin{cases} T(x) = -\dfrac{I^2R_{\mathrm{e}}R_{\mathrm{t}}}{2h^2}x^2 + C_1x + C_2 \\ C_1 = \dfrac{1}{h}\dfrac{SIR_{\mathrm{t}}\left\{0.5I^2R_{\mathrm{e}}R_{\mathrm{t}}\left[1-SIf_{\mathrm{c}}R_{\mathrm{t}}+2f_{\mathrm{c}}\left(1+1/f_{\mathrm{i}}\right)\right]+T_{\mathrm{a}}\right\} - Q_{\mathrm{h}}R_{\mathrm{t}}\left(1-SIf_{\mathrm{c}}R_{\mathrm{t}}\right)}{SIR_{\mathrm{t}}\left(1-SIf_{\mathrm{c}}R_{\mathrm{t}}\right)+1+1/f_{\mathrm{i}}} \\ C_2 = \dfrac{\left(1+1/f_{\mathrm{i}}\right)\left\{0.5I^2R_{\mathrm{e}}R_{\mathrm{t}}\left[1-SIf_{\mathrm{c}}R_{\mathrm{t}}+2f_{\mathrm{c}}\left(1+1/f_{\mathrm{i}}\right)\right]+T_{\mathrm{a}}\right\}+Q_{\mathrm{h}}R_{\mathrm{t}}\left[\left(1-SIf_{\mathrm{c}}R_{\mathrm{t}}\right)+f_{\mathrm{c}}\left(1+1/f_{\mathrm{i}}\right)\right]}{SIR_{\mathrm{t}}\left(1-SIf_{\mathrm{c}}R_{\mathrm{t}}\right)+1+1/f_{\mathrm{i}}} \end{cases} \tag{S8}$$

Therefore, the temperature difference between the two sides of the thermoelectric leg (ΔT) is expressed as follows

$$\Delta T = T_{\mathrm{h}} - T_{\mathrm{c}} = \frac{0.5I^2R_{\mathrm{e}}R_{\mathrm{t}}\left(1+1/f_{\mathrm{i}}\right)\left(f_{\mathrm{h}}-2SIR_{\mathrm{t}}f_{\mathrm{h}}f_{\mathrm{c}}-f_{\mathrm{c}}\right) - SIR_{\mathrm{t}}T_{\mathrm{a}}\left(f_{\mathrm{h}}+f_{\mathrm{c}}\right) + R_{\mathrm{t}}Q_{\mathrm{h}}f_{\mathrm{h}}\left(1-SIR_{\mathrm{t}}f_{\mathrm{c}}\right)}{SIR_{\mathrm{t}}\left(f_{\mathrm{h}}-SIR_{\mathrm{t}}f_{\mathrm{h}}f_{\mathrm{c}}-f_{\mathrm{c}}\right)+\left(1/f_{\mathrm{i}}+1\right)\left(f_{\mathrm{h}}-f_{\mathrm{c}}\right)+1} \tag{S9}$$

where T_{h} and T_{c} are the hot-side and cold-side temperatures of the thermoelectric leg, respectively. Since the complex expression, some methods need to be done to simplify Equation (S9). Note that S is usually on the order of 1×10^{-4} V K^{-1}. f_{c} is usually less than 1. Therefore, the sum term $1\text{-}2SIR_{\mathrm{t}}f_{\mathrm{c}}$ and $1\text{-}SIR_{\mathrm{t}}f_{\mathrm{c}}$ is considered approximately equal to 1. This simplified approach was also used by Zhu Kang et al. in dealing with the efficiency model[1, 2]. Therefore, Equation (S9) is abbreviated as follows

$$\Delta T \approx \frac{0.5I^2R_{\mathrm{e}}R_{\mathrm{t}}\left(1+1/f_{\mathrm{i}}\right)\left(f_{\mathrm{h}}-f_{\mathrm{c}}\right) - SIR_{\mathrm{t}}T_{\mathrm{a}}\left(f_{\mathrm{h}}+f_{\mathrm{c}}\right) + R_{\mathrm{t}}Q_{\mathrm{h}}f_{\mathrm{h}}\left(1-SIR_{\mathrm{t}}f_{\mathrm{c}}\right)}{SIR_{\mathrm{t}}\left(f_{\mathrm{h}}-f_{\mathrm{c}}\right)+\left(1/f_{\mathrm{i}}+1\right)\left(f_{\mathrm{h}}-f_{\mathrm{c}}\right)+1} \tag{S10}$$

Then, to further derive, the definition of I, power (P), efficiency (η), the ratio of load resistance (R_{L}) to R_{e} (m), figure-of-merit (Z) need to be shown as follows

$$I = \frac{S\left(T_\mathrm{h} - T_\mathrm{c}\right)}{R_\mathrm{e} + R_\mathrm{L}} \tag{S11}$$

$$P = I^2 R_\mathrm{L} \tag{S12}$$

$$\eta = \frac{P}{Q_\mathrm{h}} \tag{S13}$$

$$m = \frac{R_\mathrm{L}}{R_\mathrm{e}} \tag{S14}$$

$$Z = \frac{S^2\sigma}{\kappa} = \frac{PF}{\kappa} \tag{S15}$$

where *PF* is the power factor. Substitute Equations (S11), (S12), (S13), (S14), and (S15) into Equation (S10) to obtain efficiency expression.

$$\begin{cases} \eta = \dfrac{P}{Q_\mathrm{h}} = \dfrac{2ZR_\mathrm{t}Q_\mathrm{h} f_\mathrm{h}^2 m}{a_1^2 + a_2 + a_1\sqrt{a_1^2 + 2a_2}} & (a) \\ a_1 = \left[\left(1/f_\mathrm{i} + 1\right)\left(f_\mathrm{h} + f_\mathrm{c}\right) + 1\right]\left(m+1\right) + Z\left[T_\mathrm{a}\left(f_\mathrm{h} + f_\mathrm{c}\right) + R_\mathrm{t}Q_\mathrm{h} f_\mathrm{h} f_\mathrm{c}\right] & (b) \\ a_2 = ZR_\mathrm{t}Q_\mathrm{h} f_\mathrm{h}\left(f_\mathrm{h} - f_\mathrm{c}\right)\left(2m + 1 - 1/f_\mathrm{i}\right) & (c) \end{cases} \tag{S16}$$

By numerical analysis, we found the $a_1^2+a_2 \approx a_1(a_1^2+2a_2)^{0.5}$. Figure S8 shows the ratio of $a_1^2+a_2$ to $a_1(a_1^2+2a_2)^{0.5}$ equals to 1 with the range of $q_\mathrm{h}\cdot h$ =1-1000 W m^{-1}, T_a=300-450 K, f_h=1-1000, f_c=0.01-10, f_i=0.1-100, and m=0.4-10. Besides, the properties of six thermoelectric materials at 300 K are also used to verify this conclusion. The chosen thermoelectric materials are p-SiGe[3], p-MgAgSb[4], p-half-Heusler[5], n-CoSb[6], n-MgSnGe[7] and n-BaGaSn[8], respectively. Detailed material properties are shown in Figure S1. Therefore, Equation (S16) is abbreviated as follows

$$\eta = \frac{ZR_\mathrm{t}Q_\mathrm{h} f_\mathrm{h}^2 m}{a_1^2 + a_2} \tag{S17}$$

Then, solve $\partial\eta/\partial m$=0, neglecting the meaningless negative solution to get the optimal value of m.

$$m_\mathrm{opt} = \frac{\sqrt{\left\{\left(1/f_\mathrm{i}+1\right)\left(f_\mathrm{h}+f_\mathrm{c}\right)+1+Z\left[T_\mathrm{a}\left(f_\mathrm{h}+f_\mathrm{c}\right)+R_\mathrm{t}Q_\mathrm{h} f_\mathrm{h} f_\mathrm{c}\right]\right\}^2 + ZR_\mathrm{t}Q_\mathrm{h} f_\mathrm{h}\left(f_\mathrm{h}-f_\mathrm{c}\right)\left(1-1/f_\mathrm{i}\right)}}{\left(1/f_\mathrm{i}+1\right)\left(f_\mathrm{h}+f_\mathrm{c}\right)+1} \tag{S18}$$

We numerically analyzed the value of $[(1/f_\mathrm{i}+1)(f_\mathrm{h}+f_\mathrm{c})+1+Z[T_\mathrm{a}(f_\mathrm{h}+f_\mathrm{c})+R_\mathrm{t}Q_\mathrm{h}f_\mathrm{h}f_\mathrm{c}]]^2$ and $ZR_\mathrm{t}Q_\mathrm{h}f_\mathrm{h}(f_\mathrm{h}-f_\mathrm{c})(1-1/f_\mathrm{i})$ within the range of $q_\mathrm{h}\cdot h$ =1-1000 W m^{-1}, T_a=300-450 K, f_h=1-1000, f_c=0.01-10, f_i=0.1-100. Figure S9 shows that $[(1/f_\mathrm{i}+1)(f_\mathrm{h}+f_\mathrm{c})+1+Z[T_\mathrm{a}(f_\mathrm{h}+f_\mathrm{c})+R_\mathrm{t}Q_\mathrm{h}f_\mathrm{h}f_\mathrm{c}]]^2$ is greater than $ZR_\mathrm{t}Q_\mathrm{h}f_\mathrm{h}(f_\mathrm{h}-f_\mathrm{c})(1-1/f_\mathrm{i})$ within the investigated range. Therefore, Equation

(S18) is abbreviated as follows

$$m_{\mathrm{opt}} \approx 1+\frac{Z\left[T_{\mathrm{a}}\left(f_{\mathrm{h}}+f_{\mathrm{c}}\right)+R_{\mathrm{t}} Q_{\mathrm{h}} f_{\mathrm{h}} f_{\mathrm{c}}\right]}{\left(1 / f_{\mathrm{i}}+1\right)\left(f_{\mathrm{h}}+f_{\mathrm{c}}\right)+1} \tag{S19}$$

Substitute Equation (S19) into Equation (S16) to get our final model.

$$\begin{cases} \eta_{\max }=\dfrac{1}{g} \dfrac{\sqrt{g \cdot Z Q+1}-1}{\sqrt{g \cdot Z Q+1}+1} & (a) \\ m_{\mathrm{opt}}=1+\dfrac{Z\left[T_{\mathrm{a}}\left(f_{\mathrm{h}}+f_{\mathrm{c}}\right)+R_{\mathrm{t}} Q_{\mathrm{h}} f_{\mathrm{h}} f_{\mathrm{c}}\right]}{\left(1 / f_{\mathrm{i}}+1\right)\left(f_{\mathrm{h}}+f_{\mathrm{c}}\right)+1} & (b) \\ g=\dfrac{f_{\mathrm{h}}-f_{\mathrm{c}}}{f_{\mathrm{h}}}\left(1+\dfrac{1-1 / f_{\mathrm{i}}}{2 m_{\mathrm{opt}}}\right) & (c) \\ Z Q=\dfrac{Z R_{\mathrm{t}} Q_{\mathrm{h}} f_{\mathrm{h}}^{2}\left[\left(1 / f_{\mathrm{i}}+1\right)\left(f_{\mathrm{h}}+f_{\mathrm{c}}\right)+1\right]^{-1}}{\left(1 / f_{\mathrm{i}}+1\right)\left(f_{\mathrm{h}}+f_{\mathrm{c}}\right)+1+Z\left[T_{\mathrm{a}}\left(f_{\mathrm{h}}+f_{\mathrm{c}}\right)+R_{\mathrm{t}} Q_{\mathrm{h}} f_{\mathrm{h}} f_{\mathrm{c}}\right]} & (d) \end{cases} \tag{S20}$$

Q_{h} is expressed as follows

$$Q_{\mathrm{h}}=q_{\mathrm{h}} A \tag{S21}$$

where q_{h} is the heat flux. Therefore, by substituting (S21) into Equation (S20), we got another expression of our model.

$$\begin{cases} \eta_{\max }=\dfrac{1}{g} \dfrac{\sqrt{g \cdot Z Q+1}-1}{\sqrt{g \cdot Z Q+1}+1} & (a) \\ m_{\mathrm{opt}}=1+\dfrac{P F f_{\mathrm{i}}\left[\kappa T_{\mathrm{a}}\left(f_{\mathrm{h}}+f_{\mathrm{c}}\right)+q_{\mathrm{h}} h f_{\mathrm{h}} f_{\mathrm{c}}\right]}{\kappa^{2}\left(1+f_{\mathrm{i}}\right)\left(f_{\mathrm{h}}+f_{\mathrm{c}}\right)+\kappa^{2} f_{\mathrm{i}}} & (b) \\ g=\dfrac{f_{\mathrm{h}}-f_{\mathrm{c}}}{f_{\mathrm{h}}}\left(1+\dfrac{f_{\mathrm{i}}-1}{2 m_{\mathrm{opt}} f_{\mathrm{i}}}\right) & (c) \\ Z Q=\dfrac{P F q_{\mathrm{h}} h f_{\mathrm{h}}^{2} f_{\mathrm{i}}^{2}\left[\left(1+f_{\mathrm{i}}\right)\left(f_{\mathrm{h}}+f_{\mathrm{c}}\right)+f_{\mathrm{i}}\right]^{-1}}{\kappa^{2}\left(1+f_{\mathrm{i}}\right)\left(f_{\mathrm{h}}+f_{\mathrm{c}}\right)+\kappa^{2} f_{\mathrm{i}}+P F f_{\mathrm{i}}\left[\kappa T_{\mathrm{a}}\left(f_{\mathrm{h}}+f_{\mathrm{c}}\right)+q_{\mathrm{h}} h f_{\mathrm{h}} f_{\mathrm{c}}\right]} & (d) \end{cases} \tag{S22}$$

Note that q_{h} and h always exist simultaneously in Equation (S22). Therefore, we verified whether q_{h} and h have an equal effect in the governing Equation (S1). We selected the properties of p-MgAgSb[4] at 300 K and compared the maximum efficiency ($\eta_{\mathrm{max,num}}$) calculated by Equation (S1) with q_{h} when the product of q_{h} and h is 0.1, 1, 10, 100, and 1000 W m^{-1}, respectively, under T_{a}=300 K, f_{c}=0.1, f_{h}=10, and f_{i}=10. The variation of $\eta_{\mathrm{max,num}}$ with q_{h} is shown in Figure S10. It can be seen that when the product of q_{h} and h is the same, $\eta_{\mathrm{max,num}}$ remains unchanged, therefore, q_{h} and h have a equivalence effect. From the view of heat transfer, $\Delta T=Q_h R_t=q_h h/\kappa$. ΔT is directly related to efficiency. Therefore, if the product of q_h and h remains constant, ΔT and efficiency remain unchanged.

To find suitable thermoelectric materials for STEGs, we compare ZQ of different materials[3, 4, 6, 8-16] under different $q_h h$ when T_a = 300 K, $f_h \gg 1$, $f_c \ll 1$, and $f_i \gg 1$. We used an iteration method that was used in our previous work[2] to accurately calculate. The detailed process is shown in Figure S11. Firstly, we assume the real hot-side temperature ($T_{h,real}$) is in the range of T_a-T_a+ΔT . Secondly, we use the integral average properties between the range of T_a-T_a+ΔT to get $T_{h,eq,1}$. The detailed derivation process of $T_{h,eq}$ is shown in previous work[2]. Thirdly, we judged whether $T_{h,eq,1}$ is in the range of T_a-T_a+ΔT. If not, we further assume the $T_{h,real}$ is in the range of T_a-T_a+2ΔT and solve $T_{h,eq,2}$ again. Then we continue to judge whether $T_{h,eq,2}$ is in the range of T_a-T_a+2ΔT, and circulate the above process until $T_{h,eq,N}$ is in the range of T_a-T_a+NΔT (Each cycle N increases by 1.). If yes, we judge whether this $T_{h,eq,1}$ is within the temperature range (T_a, T_{up}) shown in the references, where T_{up} is the upper temperature limit. If not, this value cannot be used, and we should move on to the next material calculation. If yes, we think $T_{h,eq,1}$ can be regarded as the approximate value of $T_{h,real}$. Then, we can use $T_{h,real}$ as the upper-temperature limit to calculate S_{int}, σ_{int}, κ_{int}, and ZQ.

Besides, we also provide a mathematical expression of the upper limited $q_h h$ by utilizing Equation (S16) in the previous work[2]. The expression of up-limited $q_h h$ is shown as following

$$(q_h h)_{\lim} = (T_m - T_a)\kappa\left[1 + Z\frac{(1.5+ZT_a)T_m + 0.5T_a}{(2+ZT_a)^2}\right] \tag{S23}$$

where T_m is the melting temperature. We compare $(q_h h)_{lim}$ of different materials[3-6, 8-16] when T_a = 300 K, $f_h \gg 1$, $f_c \ll 1$, and $f_i \gg 1$. The integral material properties in references are used to calculate. Note that we approximately consider the maximum temperature in experimental testing as the melting point due to the lack of material property data at the melting point. Results are shown in Figure S12. Within, n-SiGe owns the highest

$(q_{\mathrm{h}}h)_{\mathrm{lim}}$ = 5495 W m^{-1}. However, the reported highest $q_{\mathrm{h}}h$ of STEGs is 2163 W m^{-1}.[17] Therefore, in Figure 3b, we only compared ZQ within $q_{\mathrm{h}}h$ = 0-2000 W m^{-1}.

Note S2. Aerogel properties

The material properties are shown in Figure S3 (b-d). It can be seen that in the solar spectrum, both samples have high light transmittances 91% (aerogel) and 87% (glass) respectively when the thickness of silica aerogel and commercial glass is 1.1 mm. The transmittance of aerogel between 0.5 μm and 1.8 μm is higher than that of commercial glass. As can be seen from Figure S3c, the transmittance of aerogel increases from 79% to 91% with the increase in catalyst dose. The thermal conductivity shows the same trend, from 34 mW m^{-1} K^{-1} to 47 mW m^{-1} K^{-1}, which is an order of magnitude difference compared to common filling materials such as polydimethylsiloxane (250 mW m^{-1} K^{-1}). This excellent light transmission and heat insulation properties are attributed to the internal nanoscale pores. BET surface area analysis of 4 mM samples showed that the average internal pore size of the aerogel was 13 nm (Figure S3d). For thermal properties, when the pore diameter in the solid is less than the mean free path of the gas molecules, the collision frequency between the gas molecules and the molecules that make up the pore diameter decreases, and the heat transferred through the gas molecules will decrease. Therefore, the pore size of 13 nm greatly reduces the thermal conductivity of the aerogel. For optical properties, the pores of nanoparticles inside the aerogel are similar in size to particles in the air, so it is transparent.

Note S3. Model modification of heat-concentrated aerogel-encapsulated STEG

Based on Equation (S22), this section revises the equations for the heat-concentrated aerogel-encapsulated STEG (a-STEG). According to the structure of heat-concentrated a-STEG, the variables involved in Equation (S22) (f_i, f_h, f_c, and q_h) are specifically expressed as follows

$$\begin{cases} f_{\mathrm{h}} = \dfrac{R_{\mathrm{h}}}{R_{\mathrm{t}}} = \dfrac{h_{\mathrm{aer}} A\kappa}{A_{\mathrm{aer}}\kappa_{\mathrm{aer}} h} = \dfrac{h_{\mathrm{aer}}\kappa}{C_{\mathrm{th}} h \kappa_{\mathrm{aer}}} & (a) \\ f_{\mathrm{i}} = \dfrac{A\kappa}{A_i \kappa_i} = \dfrac{\kappa}{(C_{\mathrm{th}}-1)\kappa_i} \approx \dfrac{\kappa}{C_{\mathrm{th}}\kappa_i} & (b) \\ f_{\mathrm{c}} = 0 & (c) \\ q_{\mathrm{h}} = C_{\mathrm{th}} q_{\mathrm{s}} e^{-\alpha h_{\mathrm{aer}}} \alpha_{\mathrm{rec}} & (d) \end{cases} \tag{S24}$$

where h_{aer} is the height of aerogel, A_{aer} is the area of aerogel, κ_{aer} is the thermal conductivity of aerogel, C_{th} is the ratio of the area of absorber to thermoelectric leg, i.e. heat-concentration coefficient, A_i is the area of insulation material, κ_i the thermal conductivity of insulation material, q_s is the sunlight intensity, α is the transmittance coefficient, and α_{rec} is the absorptivity of absorber. For heat-concentrated a-STEGs, the area of the absorber is equal to A_{aer}. In this experiment, the cold side is controlled by a copper plate and PID temperature controller, so the f_c of the cold side is very low. Consider manuscript demonstrates that, within certain limits, the effect of f_c on the efficiency is very low. Therefore, for the convenience of derivation, f_c is regarded as 0 in this experiment. Considering that C_{th} is generally much larger than 1[18], an approximation of f_i is performed to reduce the difficulty of derivation.

Substitute Equations (S24) into Equation (S22) to get the figure-of-merit (ZQ_{th}) for heat-concentrated a-STEG.

$$ZQ_{\mathrm{th}} = \frac{\dfrac{PF}{\kappa_{\mathrm{aer}}^2}\dfrac{h_{\mathrm{aer}}^2}{h}\dfrac{q_{\mathrm{s}} e^{-\alpha h_{\mathrm{aer}}}\alpha_{\mathrm{rec}}}{C_{\mathrm{th}}}}{\dfrac{h_{\mathrm{aer}}}{h\kappa_{\mathrm{aer}}}\left(\kappa_i + \dfrac{\kappa}{C_{\mathrm{th}}} + \dfrac{PFT_{\mathrm{a}}}{C_{\mathrm{th}}}\right)+1}\frac{1}{\dfrac{h_{\mathrm{aer}}}{h\kappa_{\mathrm{aer}}}\left(\kappa_i + \dfrac{\kappa}{C_{\mathrm{th}}}\right)+1} \tag{S25}$$

From the definition of ZQ_{th}, it can be seen that PF, q_s, and α_{rec} are positively correlated with ZQ_{th}, κ_{aer}, κ_i, κ, and T_a are negatively correlated with ZQ_{th}, and there are optimal values of C_{th}, h_{aer}, and h. In general, q_s is maintained at 1000 W m^{-2}. α_{rec} changes little, and most of the blackbody coatings reach more than 0.9 absorptivity. In this paper, the graphene coating is used, with an absorptivity of 0.95. However, the optimal values of C_{th}, h_{aer}, and h cannot be reached at the same point. Therefore, this paper considers that although the preparation of aerogel is mature, it is cumbersome, and accurate control of h_{aer} is difficult to achieve. Therefore, h is regarded as a fixed value in this section, that is, the optimal value of h relative to ZQ_{th} is not sought, but the optimal value of C_{th} and h_{aer} for ZQ_{th} is only sought. It is found that the optimal values of C_{th} and h_{aer} are obtained simultaneously. The expression is as follows

$$\begin{cases} C_{\mathrm{th,opt}} = \dfrac{h_{\mathrm{aer}}\kappa\left(1+ZT_{\mathrm{a}}\right)^{0.5}}{h_{\mathrm{aer}}\kappa_i + h\kappa_{\mathrm{aer}}} & (a) \\ h_{\mathrm{th,opt}} = \dfrac{h_{\mathrm{aer}}\left(C_{\mathrm{th}}\kappa_i+\kappa\right)^{0.5}\left(C_{\mathrm{th}}\kappa_i+T_{\mathrm{a}}PF+\kappa\right)^{0.5}}{C_{\mathrm{th}}\kappa_{\mathrm{aer}}} & (b) \end{cases} \tag{S26}$$

Note S4. Model modification of light-concentrated aerogel-encapsulated STEG

Similar to Note S3, this section revises the equations for the light-concentrated a-STEG. According to the structure of light-concentrated a-STEG, the variables involved in Equation (S22) (f_i, f_h, f_c, and q_h) are specifically expressed as follows

$$\begin{cases} f_{\mathrm{h}} = \dfrac{R_{\mathrm{h}}}{R_{\mathrm{t}}} = \dfrac{h_{\mathrm{aer}} A \kappa}{A_{\mathrm{aer}} \kappa_{\mathrm{aer}} h} = \dfrac{h_{\mathrm{aer}} \kappa}{C_{\mathrm{th}} h \kappa_{\mathrm{aer}}} & (a) \\ f_{\mathrm{i}} = \infty & (b) \\ f_{\mathrm{c}} = 0 & (c) \\ q_{\mathrm{h}} = C_{\mathrm{th}} C_{\mathrm{lt}} q_{\mathrm{s}} e^{-\alpha h_{\mathrm{aer}}} \alpha_{\mathrm{rec}} \tau & (d) \end{cases} \tag{S27}$$

where τ is the transmittance of the lens, C_{lt} is the ratio of the area of the lens to the thermoelectric leg, i.e. light-concentrated coefficient, and A_{rec} is the area of the absorber. Note that, although this section is for light-concentrated a-STEG, in the actual production process of light-concentrated a-STEG, the area of the absorber is inevitably larger than the area of the thermoelectric leg. Therefore, C_{th} still exists. However, the size of the absorber used in this section is 4 mm×8 mm, while the area of a single thermoelectric leg is 2×3.5 mm×3.5 mm. Therefore, C_{th} is only 1.3. Within the void positions, only air acts as the medium for heat conduction. The convective heat transfer capacity of air in confined space is also limited. Therefore, $1/f_i$ is considered to be equal to 0 during equation solving in this note. f_c is treated as equal to 0 as same with heat-concentrated a-STEG.

Substitute the Equation (S27) into Equation (S22), figure-of-merit (ZQ_{lt}) suitable for light-concentrated a-STEG is obtained.

$$ZQ_{\mathrm{lt}} = \frac{C_{\mathrm{th}} C_{\mathrm{lt}} q_{\mathrm{s}} e^{-\alpha h_{\mathrm{aer}}} \alpha_{\mathrm{rec}} \tau h}{\dfrac{\kappa^2}{PF}\left(1+\dfrac{C_{\mathrm{th}} h \kappa_{\mathrm{aer}}}{h_{\mathrm{aer}} \kappa}\right) + T_{\mathrm{a}} \kappa} \frac{1}{1+\dfrac{C_{\mathrm{th}} h \kappa_{\mathrm{aer}}}{h_{\mathrm{aer}} \kappa}} \tag{S28}$$

ZQ_{lt} adds two additional variables C_{lt} and τ compared with ZQ_{th}, and the remaining variables are qualitatively the same, so these remaining variables are not introduced again. To reduce light loss, a high-τ lens made of K-9 material is used in this paper. The change of C_{lt} is achieved by changing the distance between the lens and the absorber. According to the definition of Equation (S28), the three parameters of C_{th}, h_{aer}, and h

have optimal values relative to ZQ_{lt}. However, C_{th} is a constant value in this section, so the optimal value of C_{th} for ZQ_{lt} is not discussed. Here, we try to give a clearer physical image from the perspective of equation derivation. Fixed C_{th} finds the optimal solution to optimize h and h_{aer}. The derived optimal value expression is as follows

$$\begin{cases} h_{\mathrm{lt,aer,opt}} = \dfrac{1}{\alpha} \\ h_{\mathrm{lt,opt}} = \dfrac{\kappa\sqrt{1+ZT_{\mathrm{a}}}}{C_{\mathrm{th}}\kappa_{\mathrm{aer}}\alpha} \end{cases} \tag{S29}$$

Although these two variables all own optimal values. However, when we substituted the physical property parameters of aerogel, the material parameters of commercial bismuth telluride, and the system parameters to be used in this section into the efficiency Equation (S29) for numerical verification. It is found that h_{aer} does have an optimal value in the experimental range of this paper. But h doesn't exist. After calculation, the optimal value of h appears to be greater than 40 mm. The ultra-high h will cause the length-diameter ratio of the thermoelectric material to be too large, which will cause the thermoelectric material to break easily during use. Therefore, the optimal value is difficult to achieve in practical application. Therefore, h is regarded as positively correlated with ZQ_{lt} in this paper

As shown in Figure S6, as the light-concentrated coefficient increases, η first increases, and then decreases. This phenomenon is different from our prediction result. This is because of the effect of radiation heat loss. The radiation heat transfer law is expressed as follows

$$q_{\mathrm{rad}} = \varepsilon\delta\left(T_{\mathrm{h}}^{4} - T_{\mathrm{a}}^{4}\right) \tag{S30}$$

where q_{rad} is the radiation heat flux, ε is the emissivity of absorber coatings, and δ is the Stefan Boltzmann constant. When the hot-side temperature increases, the radiation from the absorber increases. This paper uses a coating made from graphene coating. Hence, we used the gray body assumption, which assumes that the emissivity of the coating is equal to the absorptivity (0.95). Therefore, the radiation heat flux is calculated as shown in

Figure S6c and d. The external radiation heat flux increases from 80 W m^{-2} to 773 W m^{-2}.

References

1. K. Zhu, B. Deng, P. X. Zhang, H. S. Kim, P. Jiang and W. S. Liu, *Energy Environ. Sci.*, 2020, **13**, 3514-3526.
2. H. Li, Y. P. Wang, K. Zhu, Z. J. Han, X. Z. Wu, S. H. Wang, W. Q. Zhang and W. S. Liu, *Adv. Sci.*, 2023, **10**, 2303695.
3. G. Joshi, H. Lee, Y. C. Lan, X. W. Wang, G. H. Zhu, D. Z. Wang, R. W. Gould, D. C. Cuff, M. Y. Tang, M. S. Dresselhaus, G. Chen and Z. F. Ren, *Nano Lett.*, 2008, **8**, 4670-4674.
4. H. Z. Zhao, J. H. Sui, Z. J. Tang, Y. C. Lan, Q. Jie, D. Kraemer, K. McEnaney, A. Guloy, G. Chen and Z. F. Ren, *Nano Energy*, 2014, **7**, 97-103.
5. X. Yan, W. S. Liu, S. Chen, H. Wang, Q. Zhang, G. Chen and Z. F. Ren, *Adv. Energy Mater.*, 2013, **3**, 1195-1200.
6. X. Shi, J. Yang, J. R. Salvador, M. Chi, J. Y. Cho, H. Wang, S. Bai, J. Yang, W. Zhang and L. Chen, *J. Am. Chem. Soc*, 2011, **133**, 7837-7846.
7. W. S. Liu, H. S. Kim, S. Chen, Q. Jie, B. Lv, M. L. Yao, Z. S. Ren, C. P. Opeil, S. Wilson, C. W. Chu and Z. F. Ren, *Proc. Natl. Acad. Sci.*, 2015, **112**, 3269-3274.
8. Y. Saiga, B. Du, S. K. Deng, K. Kajisa and T. Takabatake, *J. Alloys Compd.*, 2012, **537**, 303-307.
9. S. I. Kim, K. H. Lee, H. A. Mun, H. S. Kim, S. W. Hwang, J. W. Roh, D. J. Yang, W. H. Shin, X. S. Li, Y. H. Lee, G. J. Snyder and S. W. Kim, *Science*, 2015, **348**, 109-114.
10. L. S. Mao, Y. N. Yin, Q. Zhang, G. Q. Liu, H. X. Wang, Z. Guo, H. Y. Hu, Y. K. Xiao, X. J. Tan and J. Jiang, *Energy Environ. Sci.*, 2020, **13**, 616-621.
11. L. D. Zhao, G. J. Tan, S. Q. Hao, J. Q. He, Y. L. Pei, H. Chi, H. Wang, S. K. Gong, H. B. Xu, V. P. Dravid, C. Uher, G. J. Snyder, C. Wolverton and M. G. Kanatzidis, *Science*, 2016, **351**, 141-144.
12. Y. He, T. Day, T. Zhang, H. Liu, X. Shi, L. Chen and G. J. Snyder, *Adv. Mater.*,

2014, **26**, 3974-3978.

13. M. Zhou, J. F. Li and T. Kita, *J. Am. Chem. Soc*, 2008, **130**, 4527-4532.
14. Q. Zhang, E. K. Chere, K. McEnaney, M. Yao, F. Cao, Y. Ni, S. Chen, C. Opeil, G. Chen and Z. Ren, *Adv. Energy Mater.*, 2015, **5**, 1401977.
15. B. Zhu, X. X. Liu, Q. Wang, Y. Qiu, Z. Shu, Z. T. Guo, Y. Tong, J. Cui, M. Gu and J. Q. He, *Energy Environ. Sci.*, 2020, **13**, 2106-2114.
16. B. Yu, M. Zebarjadi, H. Wang, K. Lukas, H. Wang, D. Wang, C. Opeil, M. Dresselhaus, G. Chen and Z. Ren, *Nano Lett.*, 2012, **12**, 2077-2082.
17. D. Kraemer, Q. Jie, K. McEnaney, F. Cao, W. S. Liu, L. A. Weinstein, J. Loomis, Z. F. Ren and G. Chen, *Nat. Energy*, 2016, **1**, 16153.
18. D. Kraemer, B. Poudel, H. P. Feng, J. C. Caylor, B. Yu, X. Yan, Y. Ma, X. Wang, D. Wang, A. Muto, K. McEnaney, M. Chiesa, Z. Ren and G. Chen, *Nat. Mater.*, 2011, **10**, 532-538.

Figures

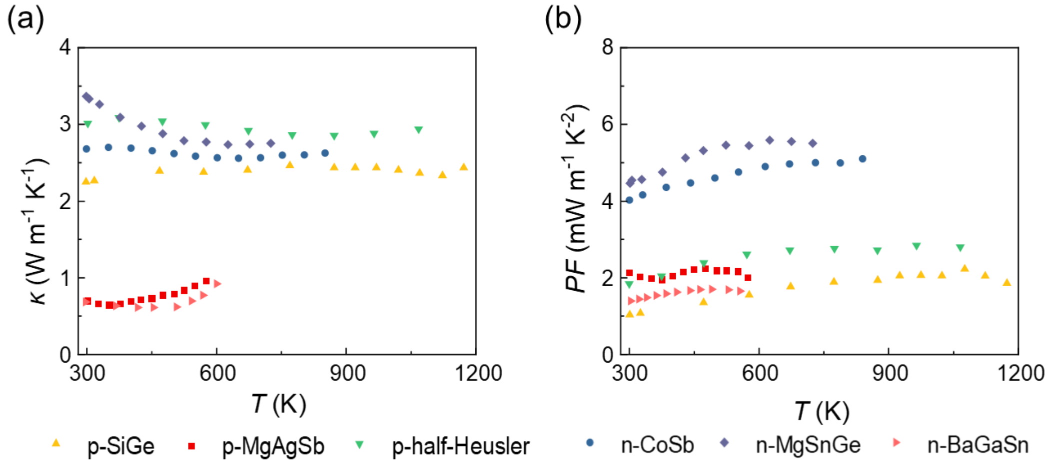

Figure S1 (a) The thermal conductivity (κ) and (b) power factor (PF) of six thermoelectric materials, including p-SiGe[3], p-MgAgSb[4], p-half-Heusler[5], n-CoSb[6], n-MgSnGe[7], and n-BaGaSn[8].

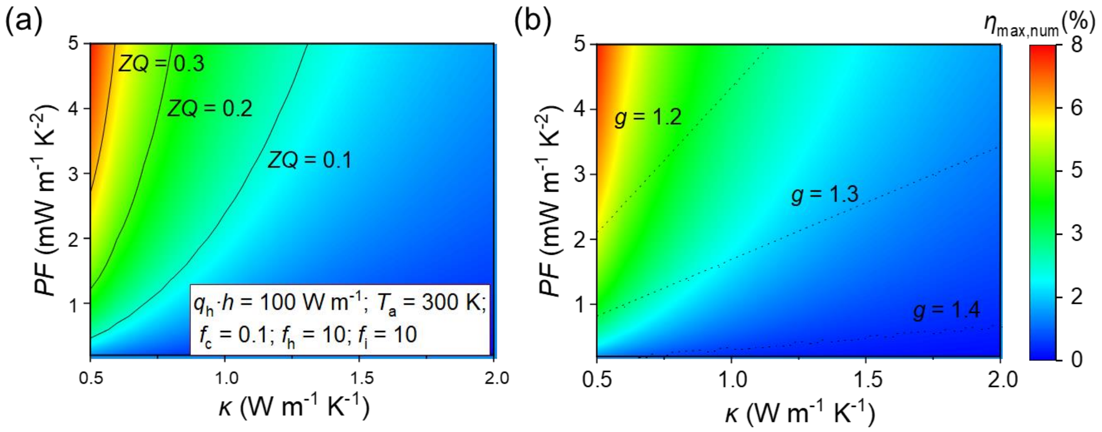

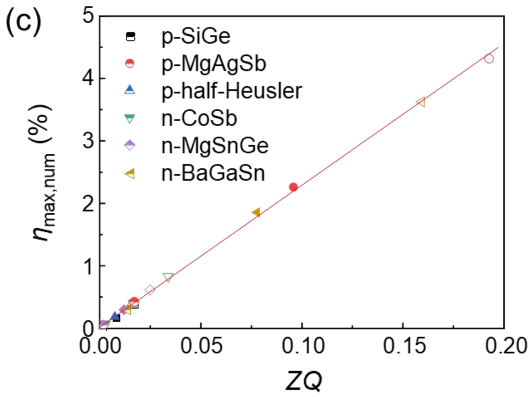

	$q_h \cdot h$ (kW m^{-1})	T_a (K)	f_c	f_h	f_i
Half-up symbols	10	300	0.1	10	10
Solid symbols	50	350	0.05	50	20
Open symbols	100	400	0.01	100	100

Figure S2 Two-dimensional plots of the maximum generation efficiency numerically calculated from the governing equation ($\eta_{max,num}$) versus the power factor (*PF*) and thermal conductivity (κ). Solid and dotted lines represent various contours of (a) *ZQ* and (b) *g* versus *PF* and κ, respectively.

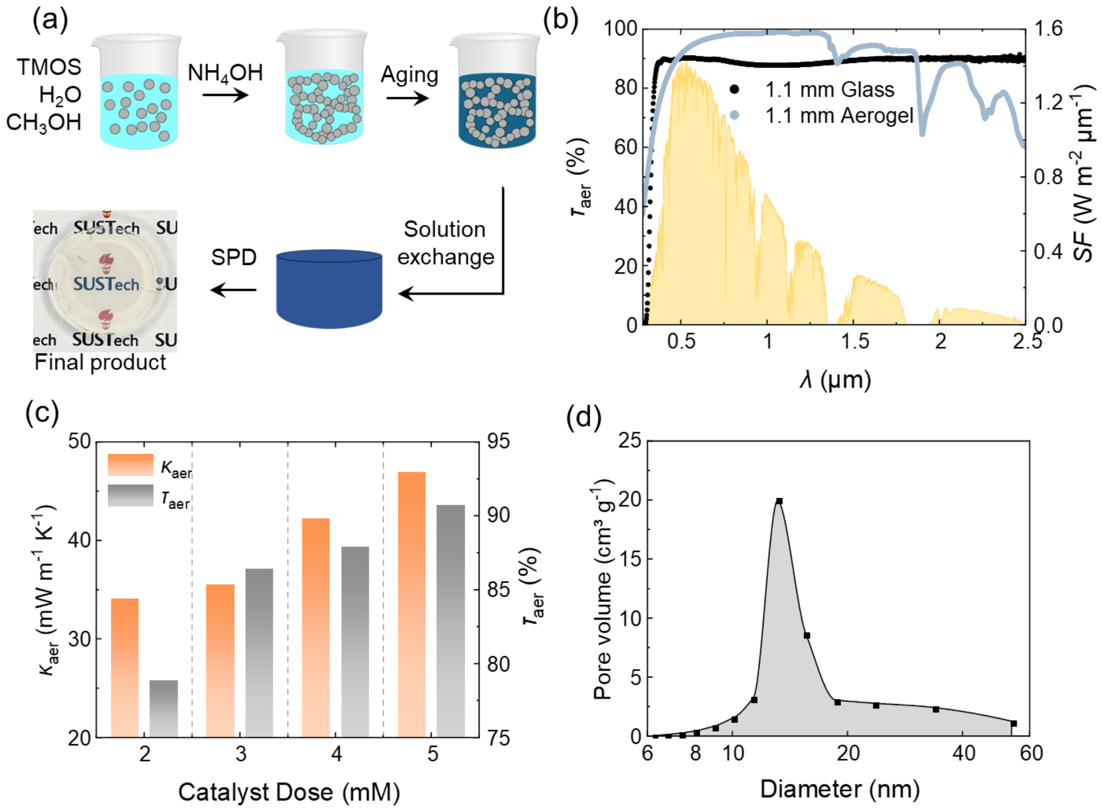

Figure S3 (a) Synthesis processes of aerogel. (b) Transmittance spectrum of a 1.1 mm thick glass and aerogel sample measured by a UV−vis−NIR spectrophotometer. (c) The thermal conductivity (κ_{aer}) and transmittance (τ_{aer}) of aerogels with different catalyst doses. (d) The distribution of pore volume versus diameter of aerogel.

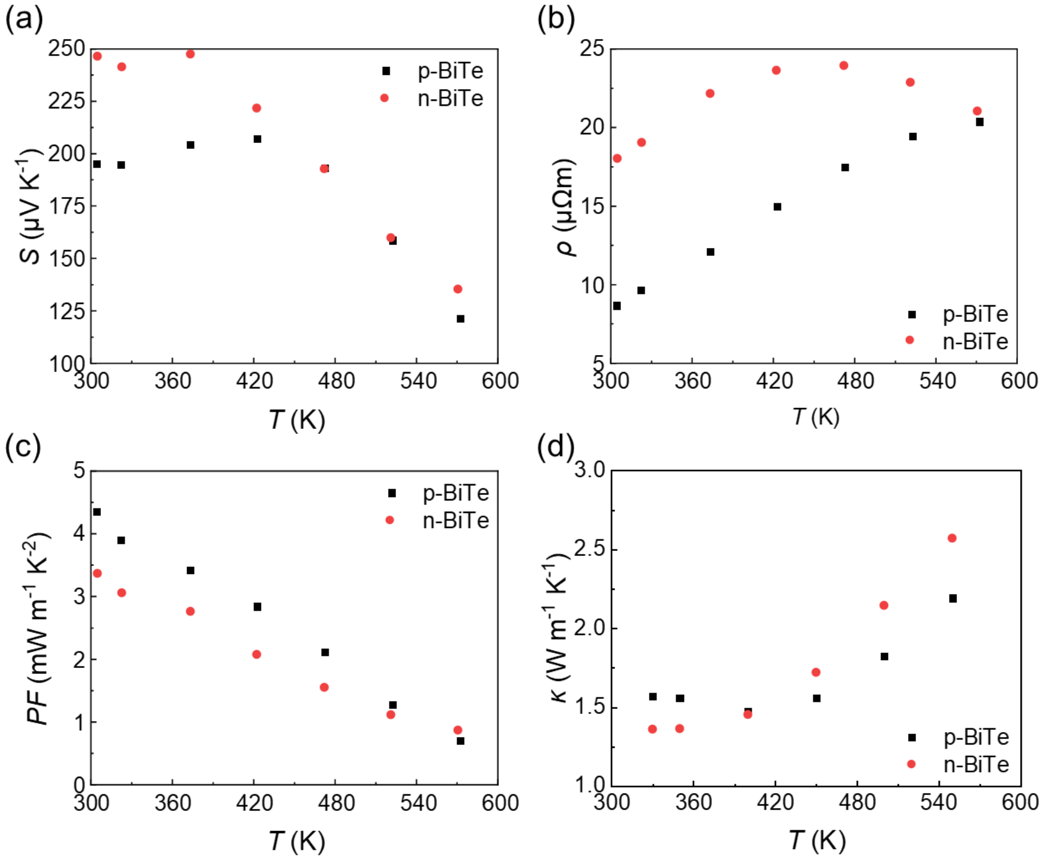

Figure S4 (a) Seebeck coefficient (*S*), (b) electrical resistivity (*σ*), (c) power factor (*PF*), and (d) thermal conductivity (*κ*) of the commercial Bi_2Te_3 used in the experiments.

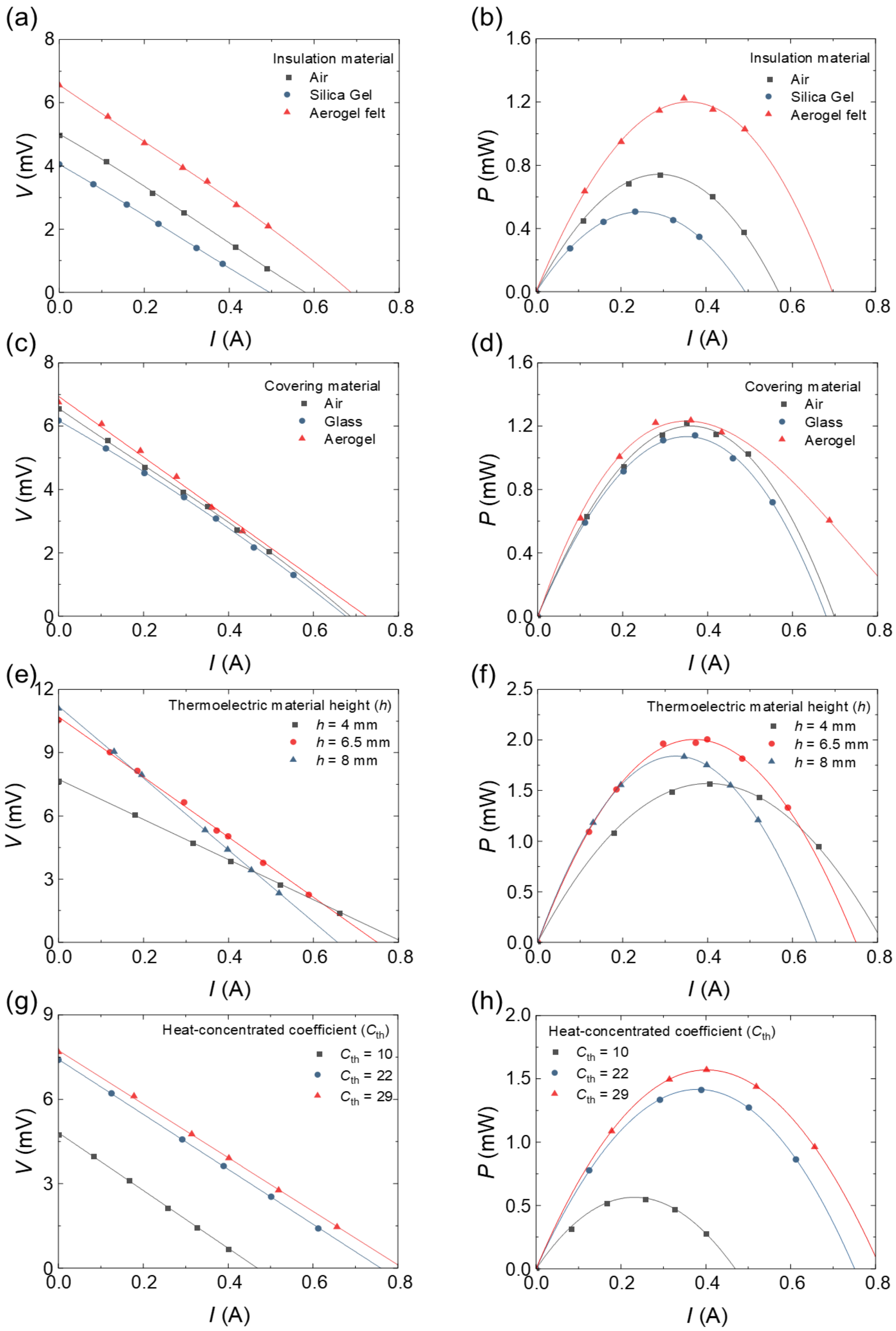

Figure S5 Voltage-current (V-I) and power-current (P-I) curves of light-concentrated aerogel-encapsulated solar thermoelectric generators under different variables. (a-b) Insulation materials. (c-d) Covering materials. (e-f) Thermoelectric material height (*h*). (g-h) Heat-concentrated coefficient (C_{th}).

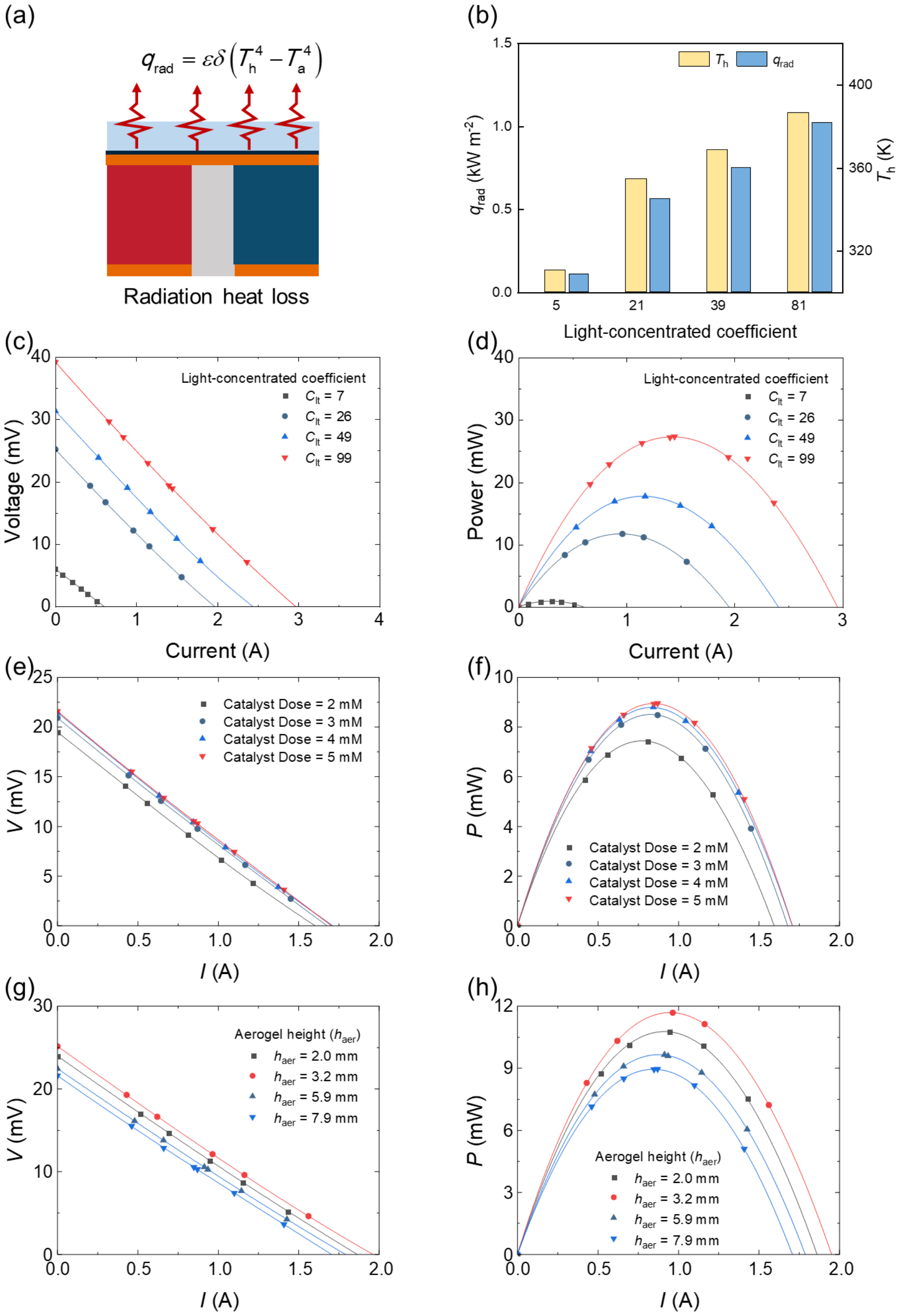

Figure S6 (a) The radiational heat loss from the hot-side of thermoelectric materials. (b) The change of hot-side temperature (T_h) and radiational heat loss (q_{rad}) with light-concentrated coefficient (C_{lt}). Voltage-current (V-I) and power-current (P-I) curves of light-concentrated aerogel-encapsulated solar thermoelectric generators under different variables (c-d) C_{lt}, (e-f) catalyst dose, (g-h) aerogel height (h_{ear}), (c-d) radiation heat flux (q_{rad}) versus C_{lt}.

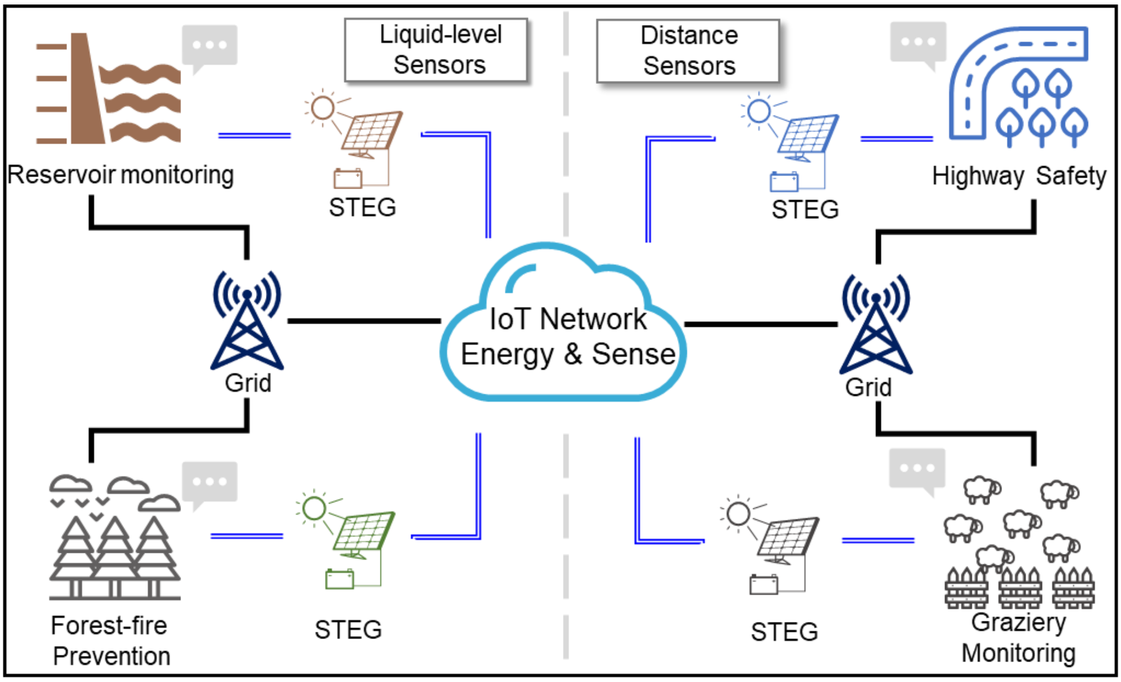

1 Figure S7 Schematic diagram of solar thermoelectric generators supplying energy to

2 Internet-of-Thing devices.

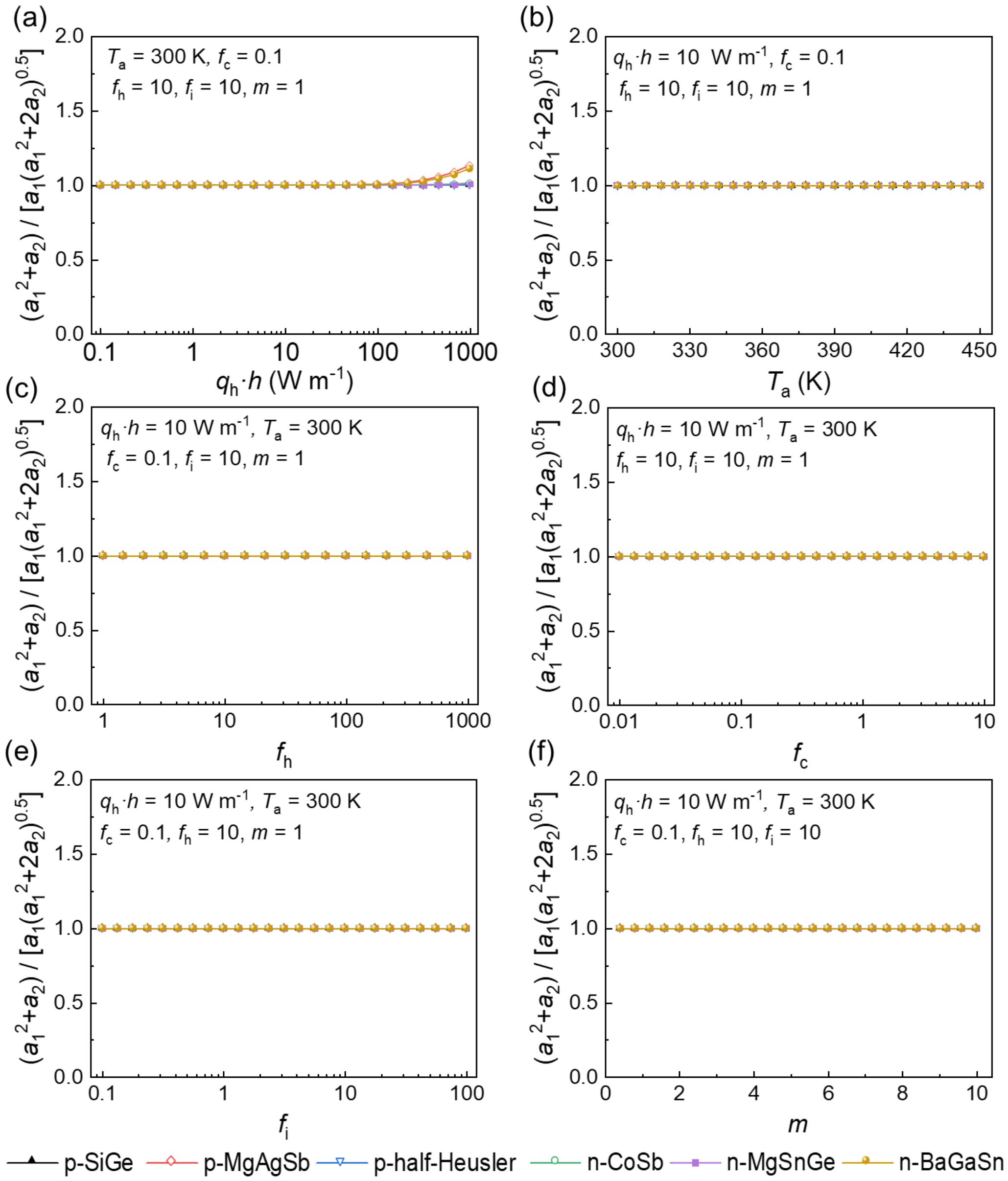

Figure S8 The ratio of $a_1^2+a_2$ to $a_1(a_1^2+2a_2)^{0.5}$ of six typical thermoelectric materials under different (a) heat flux multiplied by height of thermoelectric leg ($q_h h$), (b) ambient temperature (T_a), (c) ratio of hot-side to leg thermal resistance (f_h), (d) ratio of cold-side to leg thermal resistance (f_c) (e) ratio of insulation material to leg thermal resistance (f_i), and (f) ratio of load to internal electric resistance (m). The physical properties of thermoelectric materials[3-8] at 300 K are used.

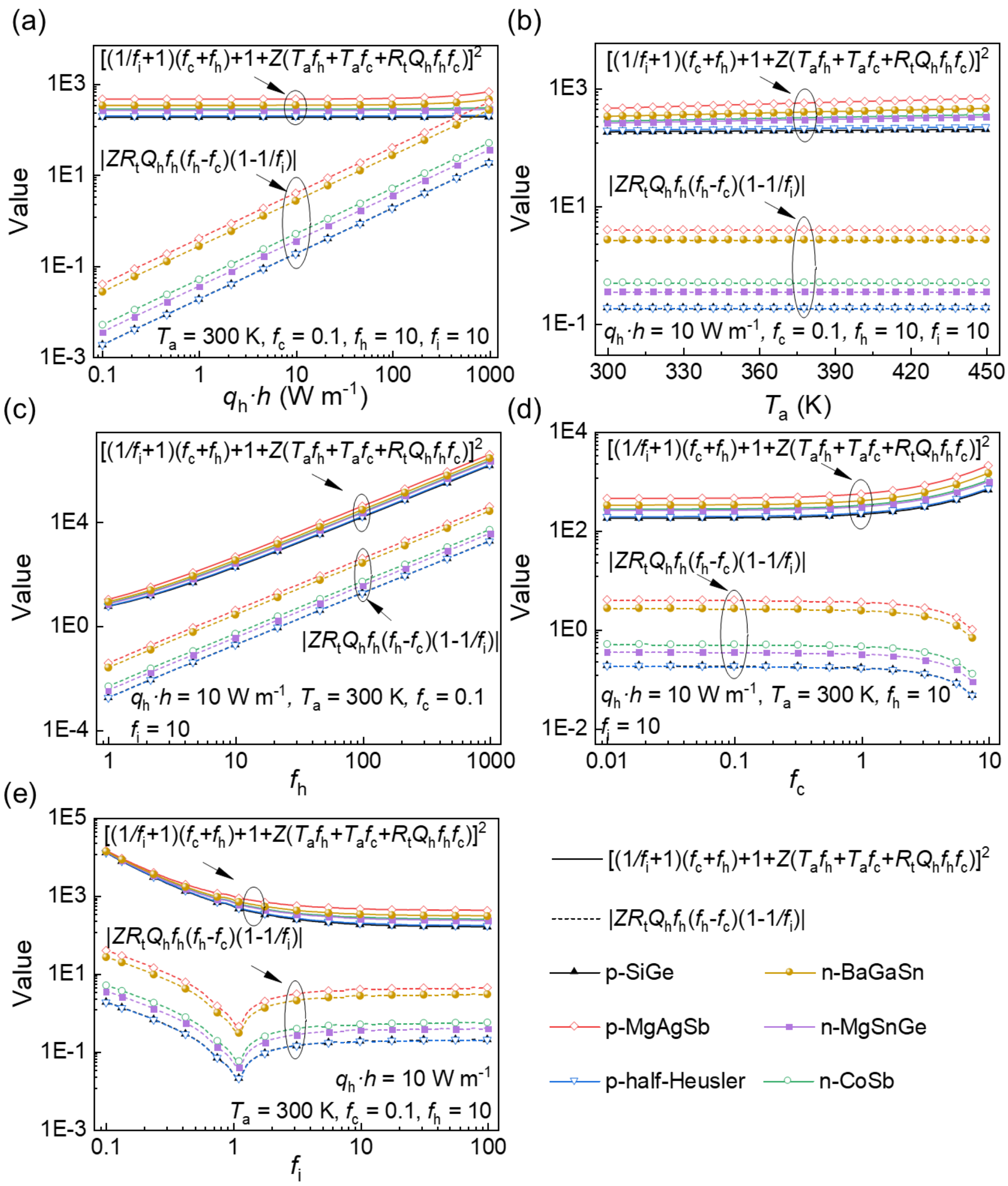

Figure S9 Values of $ZR_tQ_hf_h(f_h-f_c)(1-1/f_i)$ and $[(1/f_i+1)(f_h+f_c)+1+Z[T_a(f_h+f_c)+R_tQ_hf_hf_c]]^2$ of six typical thermoelectric materials under different (a) heat-in flux multiplied by height of thermoelectric leg (q_hh), (b) ambient temperature (T_a), (c) ratio of hot-side to leg thermal resistance (f_h), (d) ratio of cold-side to leg thermal resistance (f_c), and (e) ratio of insulation material to leg thermal resistance (f_i). The physical properties of thermoelectric materials[3-8] at 300 K are used.

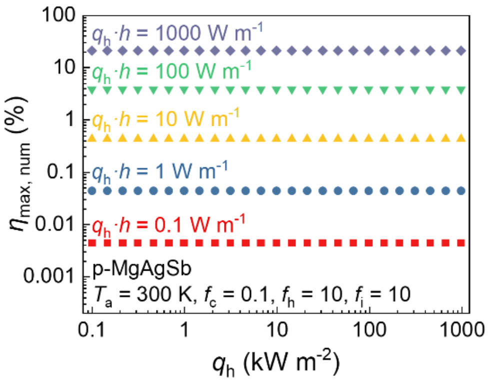

Figure S10 The maximum efficiency numerically calculated from the governing equation ($\eta_{max,num}$) with heat flux (q_h) under specific q_h multiplied by the height of the thermoelectric leg ($q_h h$). The physical properties of p-MgAgSb[4] are used.

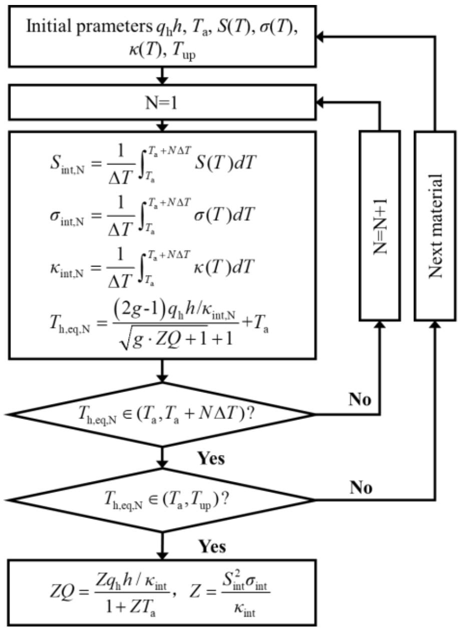

Figure S11 Flow chart of calculating the hot-side temperature by an iterative method.

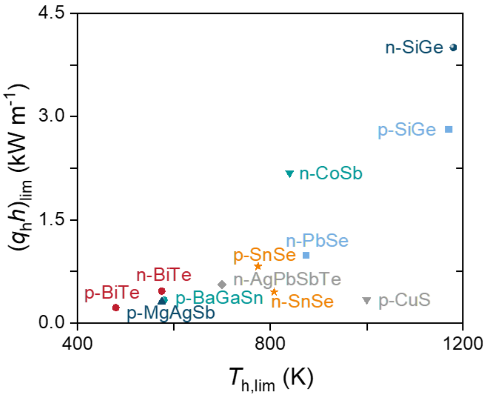

Figure S12 The up-limited values of $q_\mathrm{h}h$ and T_h for different thermoelectric materials. The material properties in references are used[3-6, 8-16].